

D-retrovirus morphogenetic switch driven by the targeting signal accessibility to Tctex-1 of dynein

Jiří Vlach*[†], Jan Lipov*[‡], Michaela Rumlová*[§], Václav Veverka*[¶], Jan Lang*^{||}, Pavel Srb*^{||}, Zdeněk Knejzlík*[‡], Iva Pichová*[§], Eric Hunter**^{††}, Richard Hrabal*[†], and Tomáš Ruml^{†§††}

*Laboratory of NMR Spectroscopy and [‡]Department of Biochemistry and Microbiology and Center of Applied Genomics, Institute of Chemical Technology, Prague, Technická 5, 16628 Prague, Czech Republic; [§]Institute of Organic Chemistry and Biochemistry, Academy of Sciences of the Czech Republic, Flemingovo nám. 2, 16610, Prague, Czech Republic; ^{||}Department of Low Temperature Physics, Faculty of Mathematics and Physics, Charles University, 18000 Prague, Czech Republic; and **Emory Vaccine Center, Yerkes National Primate Research Center, 954 Gatewood Road, Atlanta GA 30329

Edited by Peter K. Vogt, The Scripps Research Institute, La Jolla, CA, and approved May 23, 2008 (received for review February 22, 2008)

Despite extensive data demonstrating that immature retroviral particle assembly can take place either at the plasma membrane or at a distinct location within the cytoplasm, targeting of viral precursor proteins to either assembly site still remains poorly understood. Biochemical data presented here suggest that Tctex-1, a light chain of the molecular motor dynein, is involved in the intracellular targeting of Mason–Pfizer monkey virus (M-PMV) polyproteins to the cytoplasmic assembly site. Comparison of the three-dimensional structures of M-PMV wild-type matrix protein (wt MA) with a single amino acid mutant (R55F), which redirects assembly from a cytoplasmic site to the plasma membrane, revealed different mutual orientations of their C- and N-terminal domains. This conformational change buries a putative intracellular targeting motif located between both domains in the hydrophobic pocket of the MA molecule, thereby preventing the interaction with cellular transport mechanisms.

capsid assembly | dynein motor | matrix protein structure | retrovirus | transport

Gag polyproteins are major structural subunits of immature retroviral capsids and contain the determinants that mediate interactions with viral genomic RNA as well as particle assembly. The molecular mechanisms that control the accumulation of Gag molecules at the sites of assembly vary among retroviruses. Based on the assembly site, retroviruses have been shown to follow two major morphogenic pathways (1). While alpharetroviruses, gammaretroviruses, and lentiviruses (C-type retroviruses) assemble immature capsids at the inner side of the plasma membrane, the capsids of betaretroviruses (B/D-type) are formed in the cytoplasm. It has been shown that Mason–Pfizer monkey virus (M-PMV), which is the prototype of the D-type retroviruses, assembles at the pericentriolar region of an infected cell (2). Numerous studies have demonstrated that the matrix protein (MA), located at the N terminus of the Gag polyprotein, is responsible for targeting the polyprotein precursors to the site of assembly and for mediating transport of immature retroviral particles to the plasma membrane where budding occurs (3). A subtle difference in the regulation of the transport process has been suggested, as the results from several laboratories indicate that the destination of polyprotein precursors can be altered by mutations within MA. Amino acid substitutions in several domains of HIV-1 MA dramatically reduced the efficiency of particle production and redirected the majority of them to cytoplasmic vacuoles (4). Similarly, a substitution of basic for acidic residues in helix A of HIV-1 MA caused relocation of virus assembly to intracellular locations and produced normally budded noninfectious virions (5). Mutation of the N-terminal polybasic region of Moloney murine leukemia virus (Mo-MuLV) MA redirected virus assembly to the cytoplasm, suggesting a role of tryptophan residues in the intracellular transport (6).

The N terminus of MA from most retroviruses, including M-PMV, is myristoylated (7). This modification has several functions essential for the late phases of the viral life cycle. It serves as an anchor for binding Gag to the plasma membrane; provides the necessary conformation for the transport of assembled immature D-type retrovirus particles (8); and together with basic patches on the surface of MA, acts as a bipartite signal for the transport of Gag polyproteins of C-type retroviruses to the plasma membrane for assembly (9). Mutations that inhibit myristoylation or disrupt these basic patches also alter membrane binding and induce aberrant targeting of Gag to the cytoplasm or to intracellular membranes in both C- and D-type retroviruses (10). Molecular evidence for the interaction of HIV-1 Gag with membranes was provided by NMR measurements, which demonstrated that MA protein association promoted exposure of a myristate that was otherwise sequestered in the core of the molecule (10, 11). In M-PMV, the mutation blocking N-terminal Gag myristoylation does not prevent intracytoplasmic assembly; however, it totally blocks the transport of assembled viral capsids to the plasma membrane (8). Despite this evidence linking Gag myristoylation to targeting of preassembled intracytoplasmic immature particles to the site of budding and release, the role of the bipartite signal in targeting M-PMV Gag polyproteins to the assembly site is likely preempted by a dominant signal that mediates intracytoplasmic assembly.

In addition to the typical modification by myristate, MA proteins of retroviruses also share striking structural similarity despite low sequence homology (12–14). All of the MA structures solved to date are predominantly formed of four closely packed α -helices that are interconnected through loops and whose mutual orientations are similar within all structures. In addition to this conserved structural motif, lentiviral MAs (HIV-1, SIV, and EIAV) contain an additional α -helix at their C-termini.

Rather dramatic phenotypic changes induced by various point mutations also suggest that MA molecules are structurally

Author contributions: J. Lang, E.H., R.H., and T.R. designed research; J.V., J. Lipov, M.R., V.V., P.S., Z.K., and R.H. performed research; J.V., J. Lipov, M.R., V.V., J. Lang, P.S., I.P., R.H., and T.R. analyzed data; and J.V., J. Lipov, E.H., R.H., and T.R. wrote the paper.

The authors declare no conflict of interest.

This article is a PNAS Direct Submission.

Data deposition Assignments of NMR chemical shifts and restraints for structure calculation of the wild-type M-PMV MA and its R55F mutant were deposited in the BioMagResBank (www.bmr.b.wisc.edu) (accession nos. 6400 and 6401, respectively). Solution structures of the proteins were deposited in the Protein Data Bank, www.rcsb.org [PDB ID codes 2F76 (wt MA) and 2F77 (R55F mutant)].

[†]J.V. and J. Lipov contributed equally to this work.

[¶]Present address: Department of Biochemistry, University of Leicester, Leicester LE1 7RH, United Kingdom.

^{††}To whom correspondence should be addressed. E-mail: ruml@vscht.cz.

This article contains supporting information online at www.pnas.org/cgi/content/full/0801765105/DCSupplemental.

© 2008 by The National Academy of Sciences of the USA

adapted to mediate several fundamental and characteristic steps of the retroviral life cycle. Perhaps the most dramatic effect on morphogenesis was demonstrated by the replacement of arginine 55 of the M-PMV MA protein with a large hydrophobic amino acid residue (i.e., tryptophan or phenylalanine), which resulted in translocation of virus particle assembly to the plasma membrane (15, 16). In this respect, the virus behaves similarly to HIV-1 and other C-type retroviruses. The arginine 55 of M-PMV resides in the cytoplasmic targeting/retention signal (CTRS) spanning 18 aa residues from Pro-43 to Gly-60. The CTRS is conserved among D-type retroviruses and serves as a dominant translocation signal that directs M-PMV Gag precursors to an intracellular assembly site. More generally, the CTRS from M-PMV Gag is able to redirect the assembly site of C-type Mo-MuLV Gag precursors from the plasma membrane to the cytoplasm (17).

In this paper we demonstrate that a component of the dynein motor machinery, Tctex-1 (also known as DYNLT1), is the interaction partner of wild-type (wt) M-PMV MA and not R55F mutant, suggesting that this interaction is responsible for different phenotypes of M-PMV carrying either the wt MA protein or its R55F mutant. The comparison of their three-dimensional structures demonstrated substantial differences in the positions of the N- and C-terminal domains and rotation of helix III along its longitudinal axis. The driving force of this structural change is the tendency of the molecule to bury the hydrophobic side chain of phenylalanine into the core of the protein, thereby preventing interaction between the CTRS and the dynein motor machinery.

Results

Tctex-1 Is Required for Pericentriolar Targeting of M-PMV Gag. The cytoplasmic targeting of M-PMV Gag is controlled by a cytoplasmic targeting/retention signal within MA domain of Gag polyprotein (17), and point mutations within this sequence convert the type D to type C morphogenesis (15). Sfakianos *et al.* showed that the intracellular destination of wt M-PMV Gag polyproteins is the pericentriolar region of the cytoplasm and indicated the involvement of dynein-dynactin motor in this process (2). Another indication that the dynein motor can be responsible for Gag transport originates from a yeast two-hybrid screening that suggested Tctex-1 (t-complex testis-expressed-1) protein, a light chain of the dynein motor complex, to be a possible interacting partner (S. S. Rhee, personal communication).

To investigate the role of Tctex-1 in the transport of M-PMV Gag to the cytoplasmic assembly site, we compared the intracellular localization of wt Gag in 293T cells expressing physiological levels of Tctex-1 with that in the cells where the production of Tctex-1 was suppressed by specific siRNA. The effect of silencing was confirmed by Western blot analysis of the siRNA-treated cells, in which Tctex-1 levels were significantly reduced compared with the untreated control (Fig. 1A). In the Tctex-1 silenced cells, targeting of Gag to the pericentriolar region was blocked and most of the precursor was found accumulated at the plasma membrane (Fig. 1B Right). This contrasts to the noticeable intracytoplasmic accumulation of Gag in cells with wt levels of Tctex-1, where most of the Gag was either concentrated near the nucleus (Fig. 1B Left) or in the punctate sites beside the concentrated Gag in the vicinity of nucleus (white arrow in Fig. 1B Center). This effect of Tctex-1 depletion indicates the important role for this protein in the pericentriolar targeting of the wt M-PMV Gag.

M-PMV wt MA Protein, in Contrast to the R55F MA Mutant, Interacts with Tctex-1 *in Vitro*. To investigate this interaction and to elucidate the effect of the R55F mutation, we incubated equal aliquots of the same lysate of *E. coli* expressing human Tctex-1 (Fig. 2A and C, lane 1) overnight with GST-Bind resin loaded with identical amounts of purified and immobilized wt or R55F MA proteins C-terminally extended with GST. Although

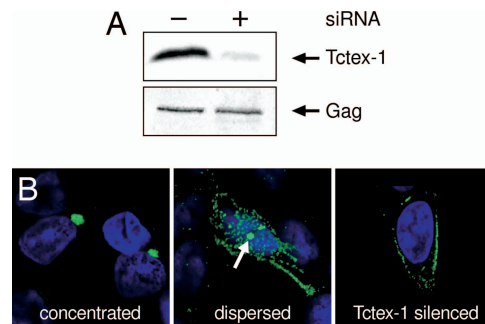


Fig. 1. The effect of Tctex-1 on localization of M-PMV wt Gag. 293T cells cotransfected by pSARM4Gag vector and Silencer siRNA for Tctex-1 (DYNLT1) were analyzed 24 h posttransfection. The cells were treated and stained with FITC conjugated antibody as described in *Materials and Methods*. Nuclei were stained by DAPI. (A) Western blot demonstrating the levels of Tctex-1 [detected by T1 mouse monoclonal antibody (Upper)] and Gag [detected by rabbit anti M-PMV MA antibodies (Lower)] in the control and Tctex-1-depleted cells, respectively. (B) Intracellular localization of M-PMV Gag in the control (Left and Center) and Tctex-1-depleted cells.

comparable amounts of wt and R55F MA were immobilized (Fig. 2A and B, lanes 2 and 3, respectively), Tctex-1 bound efficiently only to wt MA (Fig. 2C, lane 2). In contrast, no detectable amount of Tctex-1 bound to immobilized MA.R55F-GST (Fig. 2C, lane 3). No nonspecific binding of Tctex-1 to the GST-Bind resin was observed in the negative-control resin lacking immobilized MA (Fig. 2A and C, lane 4).

These results demonstrate that Tctex-1 can bind efficiently to M-PMV MA and that a point mutation in the CTRS sequence of this protein abrogates the ability of MA to bind to the Tctex-1 protein.

Replacement of Arginine 55 with Phenylalanine in the Matrix Domain Impairs the Interaction of M-PMV Gag with Tctex-1 in Mammalian Cells.

The intracellular interaction of M-PMV Gag polyprotein with Tctex-1 was investigated further by a coimmunoprecipitation experiment performed with lysates of COS-1 cells cotransfected

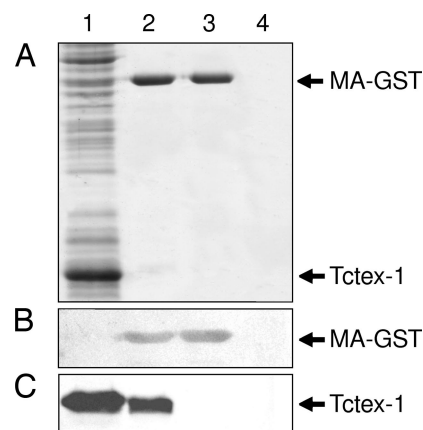


Fig. 2. The *in vitro* interaction of M-PMV wt and R55F MA with Tctex-1. The wt or R55F MA C-terminally extended with GST (MA-GST) were immobilized on GST-Bind resin (Novagen) and allowed to interact with lysates of *E. coli* BL21(DE3) cells expressing human Tctex-1. Proteins were resolved by SDS Tris-Tricine acrylamide gel electrophoresis. (A) Coomassie blue-stained gel. (B) Western blot; MA detected by rabbit anti-M-PMV MA antibody. (C) Western blot; Tctex-1, detected by rabbit anti-Tctex antibody. Lane 1, total lysate of *E. coli* BL21(DE3) after 4 h expression of Tctex-1; lane 2, binding of Tctex-1 to wt MA-GST immobilized on GST-Bind resin; lane 3, binding of Tctex-1 to MA.R55F-GST immobilized on GST-Bind resin; lane 4, Tctex-1 applied on GST-Bind resin (control of possible nonspecific Tctex-1 binding).

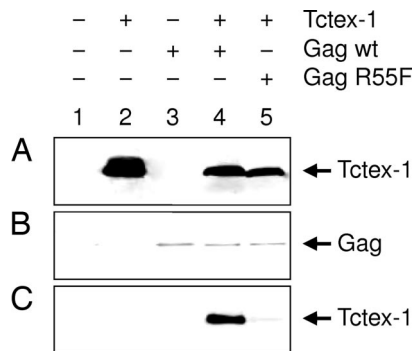


Fig. 3. The interaction of M-PMV wt and R55F Gag with human Tctex-1 in the COS-1 cells. The interaction of Gag with Tctex-1 was determined by coimmunoprecipitation from the lysate of COS-1 cells cotransfected with vectors carrying genes encoding human Tctex-1 tagged with a c-myc epitope (c-mycTctexCMV) and either wt Gag or R55F Gag as shown on top of the figure. Gag and Tctex-1 proteins were resolved by SDS/PAGE or SDS Tris-Tricine acrylamide gel electrophoresis, respectively. Rabbit anti-M-PMV CA and monoclonal anti-c-myc antibodies were used for Western blot detection of intracellular expression of Gag and Tctex-1 proteins, respectively. The complexes were immunoprecipitated with rabbit anti-CA antibody. Monoclonal anti-c-myc antibody was used for Western blot identification of immunoprecipitated Tctex-1. (A and B) Analysis of intracellular proteins. (C) Analysis of immunoprecipitated material.

with expression plasmids for production of human Tctex-1 tagged with the c-myc epitope and M-PMV wt or R55F Gag polyproteins. The molecular complexes were immunoprecipitated from the cell lysates by polyclonal antibody against capsid protein (a major immunogenic domain of Gag), and Tctex-1 interacting with the MA domain of Gag polyprotein was analyzed by Western blot using monoclonal anti-c-myc antibody. This experiment confirmed a strong interaction of Tctex-1 with the wt Gag (Fig. 3C, lane 4) compared to background levels of binding by the R55F mutant (Fig. 3C, lane 5). No detectable cross-reactivity of the antibodies was observed in the negative control (i.e., lysate from nontransfected cells; Fig. 3, lanes 1). Concentrations of the interacting partners in the samples subjected to immunoprecipitation were comparable, as indicated by Western blot analyses of Tctex-1 (Fig. 3A) and Gag proteins (Fig. 3B) of nonimmunoprecipitated samples.

The experiments described above demonstrate that the wt MA as an N-terminal domain of Gag interacts with Tctex-1, whereas the R55F MA mutant does not. The results suggest that either the amino acid motif *per se* or some structural change induced by the mutation alters the morphogenesis pathway due to the abrogation of the interaction between MA (or consequently Gag) and the dynein cargo recognition component Tctex-1.

Comparison of Structural Motifs of wt MA Protein and the R55F Mutant Reveals a Different Accessibility of the CTRS Sequence. We solved and compared the solution structures of wt and R55F MA to provide structural evidence for a CTRS-Tctex-1 interaction and to elucidate the mechanism of phenotype switching. Because the structure of the M-PMV MA previously published by Conte in 1997 (12) was deposited in the protein databank merely as a C α -trace (PDB accession code 1BAX), and no information regarding side chains was available, we solved an *ab initio* NMR structure of wt MA with a focus on a precise determination of the mutual positions of the helices, the structure of the CTRS region, and the definition of important side chains.

The secondary structure elements of both MA proteins follow the canonical structural motif described previously for matrix proteins of other retroviruses (10, 13, 14). The matrix proteins are composed of four α -helices whose positions were assessed

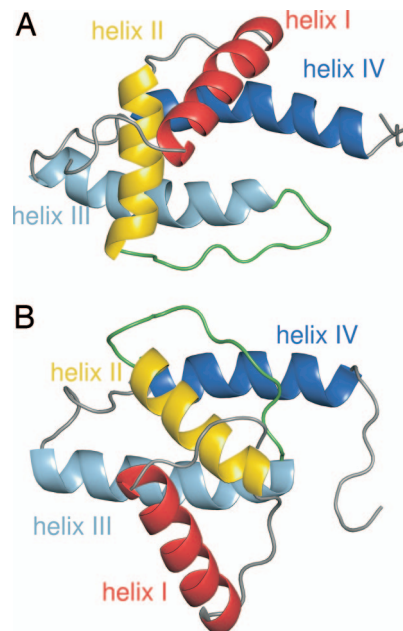


Fig. 4. Calculated structures of wt and R55F MA. Representative structures of wt MA (A) and R55F MA (B) are colored in red (helix I), yellow (helix II), light blue (helix III), and dark blue (helix IV), and the flexible loop between helices II and III is in green (residues 42–51). Structures are displayed with identical orientation of the C-terminal domain (helices III and IV). Images were created in Pymol (<http://www.pymol.org>).

from the calculated chemical shift index (18) and confirmed by complete calculation of structures [supporting information (SI) Table S1]. Helix I, spanning residues Gln-7–Thr-21, is joined to helix II through an extended loop formed by residues Arg-22–Lys-27 (Fig. 4). Helix II (residues Tyr-28–Asp-40) is terminated by a semistructured loop (Thr-41–Phe-45). Our results did not confirm the well defined 3_{10} helix in this region of the wt MA reported previously by Conte (12). The linker between helices II and III continues by a rather flexible hairpin (Phe-45–Asp-52). Numerous hydrophobic contacts have been found between helices III (residues Ile-53–Phe-70) and IV (residues Thr-78–Asp-91), which are connected by another semistructured loop formed by residues Gly-71–Val-77. Importantly, we found significant differences between the global folds of wt MA and the R55F mutant. The major difference relates to the mutual positions of their N- and C-terminal domains formed by helices I and II and helices III and IV, respectively. The reorientation of both domains can be expressed as a change of the angle between the longitudinal axes of helices II and III, which is 98° in the wt MA but increases to 322° in the R55F MA mutant. On the other hand, neither the angles between helices I and II nor those between helices III and IV differ substantially in the two molecules (124° vs 120° and 172° vs 175° , respectively). Another important structural difference between the molecules is a rotation of helix III of the R55F mutant along its longitudinal axis by $\approx 100^\circ$ compared to the helix III of the wt MA (see Fig. S1). These unexpected and relatively large changes in the global folds of both molecules are documented by comparison of ^1H and ^{15}N chemical shifts (Fig. S2) and confirmed by measurements of ^1H – ^{15}N residual dipolar couplings (RDCs) and validation of the calculated structures against them (Fig. S3).

The determinant of these structural changes is the replacement of the hydrophilic side chain of Arg-55 by a bulky and highly hydrophobic phenylalanine. The side chain of Arg-55 in the wt MA protrudes out from the protein globule while the aromatic side chain of Phe-55 in the mutant is buried in the core of the

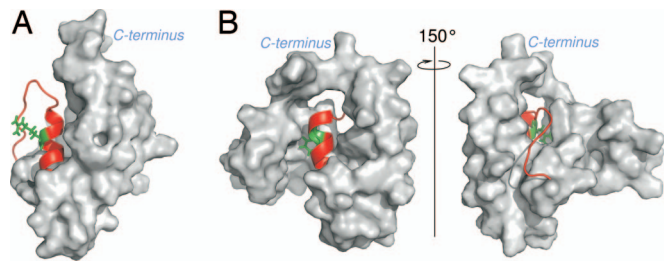


Fig. 5. Different accessibility of CTRS sequence in wt MA (A) and R55F MA (B). CTRS sequence (residues 43–60) is shown as a red ribbon and the rest of the proteins as a gray van der Waals surface; residues 55 (Arg in wt MA and Phe in R55F MA) are represented as green side-chain structures. C-terminal domains (helices III and IV) are oriented identically in both molecules.

protein as shown in Fig. 5. This is presumably driven by a need to prevent exposure of the hydrophobic side chain of Phe-55 to the solvent. This lowering of the free energy of the molecule through the hydrophobic effect results not only in the rotation of helix III but also in the reorientation of the whole C-terminal domain relative to the N-terminal domain. A result of these conformational changes is that the R55F MA CTRS is rendered inaccessible for its proposed interaction with its cellular partner.

The sets of superimposed structures of both molecules showed a large scatter in the region between residues Cys-42 and Ile-51, which is the linker between helices II and III (Fig. S4). This is also documented by comparison of positional pairwise RMSD values for the backbone heavy atoms between the well ordered parts (helices I, II, III, and IV), which were 0.69 Å for the wt or 0.85 Å for R55F, and values for the linker, which dropped to 2.38 Å or 1.36 Å, respectively. The results of a study of backbone dynamics by measurement of relaxation behavior of ^{15}N nuclei confirmed that this loop (residues 42–51) together with both termini represent the most flexible parts in the structures of both proteins. However, the flexibility of this region expressed as the order parameters S^2 of the individual peptide H-N bonds (order parameter equals 1 for absolutely rigid bond and 0 for totally flexible one, data shown in Fig. S5) is different for wt and R55F MA, especially in the Gln-47-Arg/Phe-55 region. Although the whole region (Phe-44 – Arg-55) is rather flexible in the wt structural motif (average $S^2 \approx 0.60$), the amino acid residues following Thr-50 in the R55F mutant are significantly more rigid ($S^2 \approx 0.85$). This finding supports the structural data demonstrating that residues Gln-47–Phe-55 of the CTRS sequence are buried into the core of the R55F molecule, which would limit their flexibility (Fig. 5).

Discussion

In this article we define an interaction partner of the M-PMV matrix protein that is likely responsible for intracellular trafficking of Gag polyproteins to the pericentriolar site of assembly. We also provide structural data for a functional link between the surface exposure of the CTRS and its role as a dominant targeting motif via interaction with dynein molecular motors. This provides a structural mechanism for the phenotypic switch between intracellular assembly of wt M-PMV Gag and membrane assembly for the R55F mutant.

Numerous mutagenesis studies have demonstrated the key role of the MA domain in the intracellular targeting and transport of the Gag polyproteins of various retroviruses. Despite the remarkable similarity of the retroviral MA structures solved to date, the destinations to which Gag molecules are targeted vary. The biochemical data presented here demonstrate that the wt M-PMV MA interacts with Tctex-1, a light chain of the multisubunit dynein molecular motor, which was shown to be responsible for recruiting cargos for retrograde protein transport (19). This finding supports the concept that the CTRS is recognized

by the dynein motor machinery for retrograde transport of Gag-synthesizing polysomes, as initially suggested by Sfakianos and Hunter (20). They reported that pericentriolar accumulation of Gag is dependent on intact microtubule-mediated transport and showed that both microtubule disruption by nocodazole, as well as over-expression of the dynein motor component dynamitin, blocked the pericentriolar accumulation of Gag. This finding is also consistent with the fact that Tctex-1 was a prominent M-PMV MA interacting partner in the yeast two-hybrid screening of a HeLa cDNA library (S. S. Rhee, personal communication).

We have verified that the ability of Gag to interact with Tctex-1 in the cell lysate depended on the presence of the basic arginine at position 55 in the matrix domain of M-PMV Gag and that the R55F mutation abrogated this interaction. The pull-down experiment demonstrated the interaction of purified wt MA-GST fusion protein with Tctex-1, and this interaction was confirmed in the context of the intact Gag polyprotein by coimmunoprecipitation experiments. The role of Tctex-1 in targeting of M-PMV Gag to the cytoplasmic assembly site was confirmed by a silencing experiment in which Tctex-1 was depleted by specific siRNA in the 293T cells. Targeting to the pericentriolar regions was efficiently blocked in the silenced cells and Gag was redirected to the plasma membrane (Fig. 1B Right). In contrast, we observed concentrated Gag localized near the nucleus and in some cases punctate staining in cells expressing normal levels of Tctex-1 (Fig. 1B Middle), reminiscent of data previously described by Sfakianos and Hunter for M-PMV wt Gag (2).

We also attempted to further characterize the MA–Tctex-1 interaction by mapping chemical shift changes of MA induced on Tctex-1 binding. However, the titration of isolated ^{15}N -labeled wt MA with isolated recombinant Tctex-1 did not yield expected shifts within the MA spectrum. Moreover, in contrast to the Tctex-1-containing cell lysate, the isolated Tctex-1 did not interact in the pull-down experiment (data not shown), suggesting that a conformational change of the Tctex-1 protein occurred during purification or that an additional cellular factor or posttranslational modification of MA might be involved in the interaction.

The solution structure of M-PMV wt MA shows that the CTRS consists of two structurally diverse moieties. The N-terminal region spanning residues Pro-43–Ile-51 forms a flexible linker between helices II and III, and due to its location at the periphery of the molecule, it is well tailored for the proposed interaction with a Tctex-1 dimer. The C-terminal half of the CTRS (residues Asp-52–Gly-60) is located at the beginning of helix III and contains an amino acid sequence Lys-54–Arg-55–Trp-56–Arg-57–Arg-58, corresponding to the motif K/R–K/R–X–X–K/R, which has been found within various proteins as a consensus motif for the interaction with Tctex-1 (21, 22).

A comparison of the structures of the wt MA and its R55F mutant shows a substantial difference in the accessibility of their respective CTRS sequences. Whereas the whole CTRS is fully displayed on the surface of the wt MA (thereby facilitating access to the dynein complex), the CTRS sequence of the R55F mutant is partially buried within the interior of the protein. Thus, in the mutant, the entire CTRS C terminus (residues Thr-50–Gly-60) would not be accessible for the interaction with Tctex-1 (Fig. 5B). Consequently, attachment to the dynein motor and transport of nascent R55F Gag proteins to their proper pericentriolar destination would be blocked. We suggest that it is the large reorientation of the whole MA domain and the limited access of the CTRS sequence that is responsible for the altered transport of Gag with the R55F mutation, rather than just the abrogation of the putative KR(55)WRR binding signal within the CTRS. This conclusion is supported by the finding that R55A mutation in M-PMV MA results in a mixture of both D- and C-type morphogenesis, in contrast to the predominantly C-type morphogenesis of the R55W or R55F mutants (C. Song and E. Hunter, unpublished results). Nevertheless, it remains possible that these

large conformational changes also interfere with the binding of other cellular components that are necessary for correct intracellular targeting of M-PMV Gag. However, the data described here and the fact that CTRS contains the Tctex-1 interaction motif (21, 22) strongly argue that it is the sequestration of the CTRS imposed by the R55F mutation that prevents the targeting of Gag, rather than other consequences of structural changes.

In summary, wt M-PMV MA, in contrast to the R55F MA, appears to interact with the dynein motor machinery through its Tctex-1 light chain. These results are consistent with the concept that the lack of interaction of the CTRS with this dynein component is responsible for the altered morphogenesis of M-PMV with a MA R55F mutation.

Comparison of the structures of wt MA and its R55F mutant demonstrated that this mutation caused not only local structural changes around the amino acid residue 55 but also global changes in protein structure, as evidenced by the reorientation of the mutual positions of the N- and C-terminal domains of the molecule and rotation of helix III by 100° along its longitudinal axis. Consequently, nascent Gag molecules bearing R55F mutation are not transported to the pericentriolar region of the cell, and an alternative transport mechanism results in the assembly of immature viral particles at the plasma membrane.

Materials and Methods

Construction of Expression Plasmids. The human Tctex-1 gene was obtained by reverse transcription of total RNA from HeLa cells and cloned into pET22b (Novagen) and pCMV-c-myc (Clontech). M-PMV gag wt and gag R55F were subcloned into pCMV (Clontech), and pSARM4 Gag was prepared by a deletion of *pro-pol-env* from the proviral vector (23). The constructs encoding GST fused to the C terminus of the MA wt and R55F were prepared in pET41a (Novagen). Bacterial plasmids for expression of pETMAPPHis and pETMAR55FPPHis, used for NMR studies, were prepared as described previously (18).

GST Pull-Down. Human Tctex-1-pET22b was expressed in *Escherichia coli* BL21 cells. The cleared lysate of the cells, lysed 4 h postinduction by lysozyme in the presence of SDS, was used for binding studies.

M-PMV MA.wt-GST and MA.R55F-GST were expressed in *E. coli* BL21 as described above. The proteins were extracted into wash/bind buffer (Novagen) and applied on GST-Bind resin. The resin was washed with three bed volumes of wash/bind buffer and then with three bed volumes of binding buffer B (25 mM Hepes, pH 7.5; 25 mM NaCl; 1% Triton X-100; 2.5 mM CaCl₂; 1 mM MgCl₂). The resin with immobilized MA wt or MA R55F protein was then incubated overnight at 4°C with the cleared lysate of *E. coli* expressing Tctex-1. The resin was then thoroughly washed with binding buffer B, resuspended in 2xSDS sample buffer, and boiled for 5 min. The bound proteins were resolved by Tris-Tricine electrophoresis and stained by Coomassie blue G-250 or blotted and detected immunochemically, by rabbit anti-M-PMV MA (RbxMPPMV MA) or rabbit anti-human Tctex-1 (RbxTctex, kindly provided by S. King).

Coimmunoprecipitation. COS-1 cells were cotransfected with c-mycTctex.pCMV and wtGag.pCMV or R55FGag.pCMV by using FuGENE 6 Reagent (Roche Applied Science). Two days post transfection, the cells were washed once with PBS and lysed in Co-IP buffer [20 mM Tris-HCl, pH 7.5; 150 mM NaCl; 1 mM EDTA; 1 mM DTT; 0.1 mM MgCl₂; 0.5% Nonidet P-40; protease inhibitor mix (Sigma)] for 15 min on ice. The cell lysate was cleared by centrifugation. One fifth of the cleared lysate for each sample was mixed with 2xSDS sample buffer and used for Western blot, with monoclonal anti-c-myc and rabbit anti-M-PMV CA antibodies. The rest of the samples of the cleared cell lysates were incubated with rabbit anti-M-PMV CA antibody overnight at 4°C, and the bound complex was precipitated by protein A for 2 h at 4°C. The pellets were washed three times with Co-IP buffer and then

once with PBS. Proteins were resolved by SDS/PAGE and electroblotted, and bound c-myc-tagged Tctex was detected using anti-c-myc antibody. Western blots were developed by using SuperSignalWest Femto (Pierce).

Tctex-1 Silencing and Immunofluorescence Microscopy. 293T cells grown on coverslips were co-transfected by pSARM4Gag vector and predesigned Silencer siRNA (#s13947, Ambion) for Tctex-1 (DYNLT1). The silencing effect was determined 24 h post transfection by SDS/PAGE and immunoblotting with T1 mouse monoclonal antibody (gift of Dr. Kevin Pfister) (24). For immunofluorescence, the cells were washed twice by preheated PBS and then fixed for 2 min with -20°C acetone. Cells were re-hydrated in PBS containing 0.1% TX-100, blocked (2% BSA in PBS) and incubated with rabbit anti-MA polyclonal antibody (prepared in our laboratory 1:100) for 1 h. Cells were washed by PBS containing 0.1% TX-100 and incubated with FITC-conjugated anti-rabbit antibody (1:300, Sigma-Aldrich) for 1 h. Nuclei were stained by DAPI.

NMR Spectroscopy. NMR data were acquired on a Bruker Avance DRX 500 spectrometer (500.13 MHz for ¹H) at 25°C, processed using NMRPipe software (25) and analyzed in Sparky. Distance restraints for structure calculations were obtained from edited (¹³C/¹⁵N) 3D NOESY spectra. ¹H chemical shifts were referenced directly to the internal standard (DSS) and ¹³C and ¹⁵N chemical shifts were referenced indirectly using ratios of NMR frequencies. ¹⁵N relaxation data (longitudinal relaxation time *T*₁, transverse relaxation time *T*₂ and heteronuclear {¹H}-¹⁵N NOE) were measured on uniformly ¹⁵N labeled samples of both proteins using a conventional set of experiments. Dynamic parameters of the backbone were derived from the experiments using the Lipari-Szabo motional model (26).

Structure Calculation of wt MA and R55F MA Proteins. The calculation of wt and R55F MA protein structures was based on interproton distance restraints derived from NOESY spectra, dihedral angles φ and ψ , and a regular hydrogen bond network. An estimate of backbone dihedral angles φ and ψ was performed in TALOS program based on ¹H α , ¹³C α , ¹³C β , ¹³C', and ¹⁵N chemical shifts. Hydrogen bond restraints were used for α -helical segments identified in later stages of computation. The Aria software package (version 2.0alpha) was initially used to calibrate NOE restraints, to assign NOESY cross peaks, and to calculate preliminary structures. Distance restraints, together with dihedral angles and hydrogen bond restraints, were then used as an input for Xplor-NIH (27), where the final sets of 100 (wt) or 50 (R55F) MA structures were calculated using standard protocol for torsion angle dynamics and simulated annealing. Distribution of φ and ψ dihedral angles in the Ramachandran core, additional allowed, generously allowed, and disallowed regions for the 20 best WT structures is (%) 88.6 ± 2.1, 9.8 ± 1.9, 1.2 ± 0.9 and 0.3 ± 0.5, respectively; and for 18 best R55F structures, 91.2 ± 1.5, 7.7 ± 1.7, 1.1 ± 1.0 and 0.1 ± 0.3.

The accuracy of calculated structures was validated by comparison of measured and back-calculated RDCs. The signal splittings of isotropic and partially aligned wt or R55F MA in 5.5% or 4.5% polyacrylamide gel, respectively, were measured by using the D5SE-¹H,¹⁵N-HSQC experiment (28), yielding one-bond ¹H-¹⁵N RDCs. The synthetic RDCs were back-calculated by singular value decomposition method from a set of eight (wt MA) or six (R55F MA) structures recalculated with RDC constraints, and correlated with the measured values (Fig. S3). The back-calculations and analyses were performed in the iDC module (29) of Igor Pro 6.0 software (<http://www.wavemetrics.com>).

ACKNOWLEDGMENTS. We thank Sung S. Rhee (U.S. Food and Drug Administration, Rockville, MD) for providing unpublished results and discussions on the role of Tctex-1 in M-PMV replication and Dr. K. Pfister (University of Virginia, Charlottesville, VA) and Dr. S. M. King (McMaster University, Hamilton, ON, Canada) for kind gifts of anti Tctex-1 monoclonal and rabbit antibody, respectively. This work was supported by Czech Ministry of Education Grants 1M6837805002, MSM 6046137305, 0021620835, and ME 904, Z 40550506; Czech Science Foundation Grants 2003/02/P098, 2003/03/0490, and SCO/06/E001; the Grant Agency of the Academy of Sciences of the Czech Republic KAN200100801; the Grant Agency of Charles University 38707; and National Institutes of Health Grant CA 27834.

- Hunter E (1994) Macromolecular Interactions in the assembly of HIV and other retroviruses. *Sem Virol* 5:71–83.
- Sfakianos JN, LaCasse RA, Hunter E (2003) The M-PMV cytoplasmic targeting-retention signal directs nascent Gag polypeptides to a pericentriolar region of the cell. *Traffic* 4:660–670.
- Freed EO (2002) Viral late domains. *J Virol* 76:4679–4687.
- Freed EO, Orenstein JM, Bucklerwhite AJ, Martin MA (1994) Single amino-acid changes in the human-immunodeficiency-virus type-1 matrix protein block virus particle-production. *J Virol* 68:5311–5320.
- Cannon PM, et al. (1997) Structure-function studies of the human immunodeficiency virus type 1 matrix protein, p17. *J Virol* 71:3474–3483.
- Soneoka Y, Kingsman SM, Kingsman AJ (1997) Mutagenesis analysis of the murine leukemia virus matrix protein: Identification of regions important for membrane localization and intracellular transport. *J Virol* 71:5549–5559.
- Bryant M, Ratner L (1990) Myristoylation-dependent replication and assembly of human immunodeficiency virus-1. *Proc Natl Acad Sci USA* 87:523–527.
- Rhee SS, Hunter E (1987) Myristylation is required for intracellular-transport but not for assembly of D-type retrovirus capsids. *J Virol* 61:1045–1053.

9. Zhou W, Parent LJ, Wills JW, Resh MD (1994) Identification of a membrane-binding domain within the amino-terminal region of human immunodeficiency virus type 1 Gag protein which interacts with acidic phospholipids. *J Virol* 68:2556–2569.
10. Tang C, et al. (2004) Entropic switch regulates myristate exposure in the HIV-1 matrix protein. *Proc Natl Acad Sci USA* 101:517–522.
11. Saad JS, et al. (2006) Structural basis for targeting HIV-1 Gag proteins to the plasma membrane for virus assembly. *Proc Natl Acad Sci USA* 103:11364–11369.
12. Conte MR, Klikova M, Hunter E, Ruml T, Matthews S (1997) The three-dimensional solution structure of the matrix protein from the type D retrovirus, the Mason-Pfizer monkey virus, and implications for the morphology of retroviral assembly. *EMBO J* 16:5819–5826.
13. Hatanaka H, et al. (2002) Structure of equine infectious anemia virus matrix protein. *J Virol* 76:1876–1883.
14. Riffel N, et al. (2002) Atomic resolution structure of Moloney murine leukemia virus matrix protein and its relationship to other retroviral matrix proteins. *Structure* 10:1627–1636.
15. Rhee SS, Hunter E (1990) A single amino acid substitution within the matrix protein of a type D retrovirus converts its morphogenesis to that of a type C retrovirus. *Cell* 63:77–86.
16. Yasuda J, Hunter E (2000) Role of matrix protein in the type D retrovirus replication cycle: Importance of the arginine residue at position 55. *Virology* 268:533–538.
17. Choi G, et al. (1999) Identification of a cytoplasmic targeting retention signal in a retroviral Gag polyprotein. *J Virol* 73:5431–5437.
18. Vlach J, et al. (2005) Letter to the editor: Assignment of H-1, C-13, and N-15 resonances of WT matrix protein and its R55F mutant from Mason-Pfizer monkey virus. *J Biomol NMR* 31:381–382.
19. Karcher RL, Deacon SW, Gelfand VI (2002) Motor-cargo interactions: The key to transport specificity. *Trends Cell Biol* 12:21–27.
20. Sfakianos JN, Hunter E (2003) M-PMV capsid transport is mediated by Env/Gag interactions at the pericentriolar recycling endosome. *Traffic* 4:671–680.
21. Mok YK, Lo KWH, Zhang MJ (2001) Structure of Tctex-1 and its interaction with cytoplasmic dynein intermediate chain. *J Biol Chem* 276:14067–14074.
22. Sugai M et al. (2003) PTH/PTH-related protein receptor interacts directly with Tctex-1 through its COOH terminus. *Biochem Biophys Res Commun* 311:24–31.
23. Song C, Hunter E (2003) Variable sensitivity to substitutions in the N-terminal heptad repeat of Mason-Pfizer monkey virus transmembrane protein. *J Virol* 77:7779–7785.
24. Lo KW, et al. (2007) Interaction of the DYNLT (TCTEX1/RP3) light chains and the intermediate chains reveals novel intersubunit regulation during assembly of the dynein complex. *J Biol Chem* 282:36871–36878.
25. Delaglio F, et al. (1995) NMRPipe: A multidimensional spectral processing system based on UNIX pipes. *J Biomol NMR* 6:277–293.
26. Lipari G, Szabo A (1982) Model-free approach to the interpretation of nuclear magnetic resonance relaxation in macromolecules. 2. Analysis of experimental results. *J Am Chem Soc* 104:4559–4570.
27. Schwieters CD, Kuszewski JJ, Tjandra N, Clore GM (2003) The Xplor-NIH NMR molecular structure determination package. *J Magn Reson* 160:65–73.
28. Cordier F, Dingley AJ, Grzesiek S (1999) A doublet-separated sensitivity-enhanced HSQC for the determination of scalar and dipolar one-bond J-couplings. *J Biomol NMR* 13:175–180.
29. Wei YF, Werner MH (2006) iDC: A comprehensive toolkit for the analysis of residual dipolar couplings for macromolecular structure determination. *J Biomol NMR* 35:17–25.